

Litmus tests of the flat Λ CDM model and model-independent measurement of $H_0 r_d$ with LSST and DESI

Benjamin L'Huillier^{},^a Ayan Mitra^{},^{b,c} Arman Shafieloo^{},^{d,e}
Ryan E Keeley^{}^f and Hanwool Koo^{}^g

^aDepartment of Physics and Astronomy, Sejong University, 05006 Seoul, Korea

^bCenter for AstroPhysical Surveys, National Center for Supercomputing Applications, University of Illinois Urbana-Champaign, Urbana, IL, 61801, USA

^cDepartment of Astronomy, University of Illinois at Urbana-Champaign, Urbana, IL 61801, USA

^dKorea Astronomy and Space Science Institute, Daejeon 34055, Korea

^eUniversity of Science and Technology, Daejeon 34113, Korea

^fUniversity of California, Merced, 5200 N Lake Road, Merced, CA 95341, USA

^gDepartment of Physics and Astronomy, University of the Western Cape, Robert Sobukwe Road, Bellville, Cape Town, 7535, South Africa

E-mail: benjamin@sejong.ac.kr, ayan@illinois.edu, shafieloo@kasi.re.kr,
rkeeley@ucmerced.edu, hanwool.koo90@gmail.com

Abstract. In this analysis we apply a model-independent framework to test the flat Λ CDM cosmology using simulated SNIa data from the upcoming Legacy Survey of Space and Time (LSST) and combined with simulated Dark Energy Spectroscopic Instrument (DESI) five-years Baryon Acoustic Oscillations (BAO) data. We adopt an iterative smoothing technique to reconstruct the expansion history from SNIa data, which, when combined with BAO measurements, facilitates a comprehensive test of the Universe's curvature and the nature of dark energy. The analysis is conducted under four different mock true cosmologies: Two curvatures ($\Omega_{k,0} = 0$ and 0.1) and two models of dark energy: a cosmological constant Λ and the phenomenologically emergent dark energy. We forecast that our reconstruction technique can constrain cosmological parameters, such as the curvature ($\Omega_{k,0}$) and $c/H_0 r_d$, with spread due to the SNIa uncertainties up to $\pm 4\%$ and ± 0.1 respectively, without assuming any form of dark energy.

ArXiv ePrint: [2407.07847](https://arxiv.org/abs/2407.07847)

Contents

1	Introduction	1
2	Theory	2
3	Data	3
3.1	Fiducial Models	3
3.2	LSST SNIa Simulations	4
3.2.1	The Rubin Observatory Legacy Survey of Space and Time (LSST)	4
3.2.2	Mock Data Generation	4
3.3	Mock BAO data from DESI 5-year	6
4	Method	6
4.1	Curvature test	7
4.2	Iterative Smoothing	8
5	Results	13
5.1	Supernova Smoothing	13
5.2	$H_0 r_d$	14
5.3	Curvature Test	15
6	Summary and Conclusion	17
A	Smooth Derivatives	17
B	Error propagation	18

1 Introduction

The concordance cosmological Λ CDM model relies on a few assumptions. Among them, homogeneity and isotropy lead to the Friedman-Robertson-Lemaître-Walker (FLRW) metric. The discovery of cosmic acceleration led to the establishment of the concordance Λ CDM model. In this model, the energy budget of the Universe today is dominated by a cosmological constant Λ , and matter by cold dark matter (CDM). The most stringent constraints on the model have been obtained by cosmic microwave background (CMB) measurements from the Planck satellite [1], baryon acoustic oscillations (BAO) [2–6] and Type Ia Supernovae (SNIa) [7–11].

The rise of tensions, in particular the Hubble tension, and the unknown nature of the main components of the model are strong hints for cosmologists to search for evidence for beyond- Λ CDM physics [12–20]. While the simplest explanation for the late-time cosmic acceleration is dark energy in the form of a cosmological constant, a dynamical DE is not excluded [21]. Recent BAO data from the Dark Energy Spectroscopic Instrument (DESI) showed evidence for a phantom dark energy or a dynamical dark energy [5]. This was further confirmed by studying physics-driven modifications of Λ CDM [22] as well as data-driven reconstructions of the expansion history [23].

Another fundamental question is the curvature of the Universe, summarized in the current curvature density parameter $\Omega_{k,0}$. The Planck 2018 (P18) data favor a negative curvature $-0.095 < \Omega_{k,0} < -0.007$ at 99% [1, 24, 25]. However, combining P18 with external data yields results consistent with a flat universe [26, 27]. Interestingly, DESI DR1 finds a preference for a small positive curvature, which disappears when combined with Planck.

Most of these constraints however are direct fits to the data assuming a particular model, typically the Λ CDM model or an extension. While this leverages the power of Bayesian statistics to provide tight constraints on the model parameters, it is important to also test the validity of the underlying hypotheses. As opposed to model-fitting, model-independent approaches provide a healthy check on the validity of a given model. Due to their extra flexibility compared to model-fitting approaches, they may also reveal the presence of unexpected features in the data and may be used to look for unaccounted for systematics [28–30].

In this work, we used a model-independent approach, namely, the iterative smoothing method, to reconstruct the expansion history from SNIa and combine it with distance measurements from BAO to perform litmus tests of the pillars of the Λ CDM model, the FLRW metric, the flatness of the Universe, and the cosmological constant, as well as to constrain $c/H_0 r_d$. Specifically, our goal is twofolds: we aim to quantify the constraining power of the combination of LSST SNIa and DESI Y5 BAO to (1) test the FLRW metric, and (2) to measure the curvature parameter and $H_0 r_d$ independently of the nature of DE.

2 Theory

In an FLRW universe, when radiation is negligible, the expansion history reads

$$h^2(z) = \frac{H^2(z)}{H_0^2} = \Omega_{m,0}(1+z)^3 + \Omega_{k,0}(1+z)^2 + (1 - \Omega_{m,0} - \Omega_{k,0})f_{\text{DE}}(z), \quad (2.1a)$$

where

$$f_{\text{DE}}(z) = \exp\left(3 \int_0^z \frac{1+w(x)}{1+x} dx\right) \quad (2.1b)$$

describes the time evolution of the dark energy density, $\Omega_{m,0}$ and $\Omega_{k,0}$ are the matter and curvature density parameters today respectively, and $w = p/\rho$ is the equation of state of dark energy. For the cosmological constant Λ , $w = -1$ and $f_{\text{DE}}(z) \equiv 1$.

The dimensionless comoving distance is defined by

$$\mathcal{D}(z) = \frac{1}{\sqrt{-\Omega_{k,0}}} \sin\left[\sqrt{-\Omega_{k,0}} \int_0^z \frac{dx}{h(x)}\right] \quad (2.2)$$

for all signs of $\Omega_{k,0}$. In particular, for $\Omega_{k,0} = 0$, eq. (2.2) simplifies to

$$\mathcal{D}(z) = \int_0^z \frac{dx}{h(x)}. \quad (2.3)$$

The angular diameter and luminosity distances are related to the comoving distance by

$$(1+z)d_A(z) = \frac{d_L(z)}{1+z} = d_M(z) = \frac{c}{H_0} \mathcal{D}(z). \quad (2.4)$$

The distance modulus from supernovae is

$$\mu(z) = 5 \log_{10} \frac{d_L}{1 \text{ Mpc}} + 25. \quad (2.5)$$

BAO, on the other hand, measure both the distances and expansion. Strictly speaking, the transverse and radial modes of the BAO give

$$\frac{d_A(z)}{r_d} = \frac{c}{H_0 r_d} \frac{\mathcal{D}(z)}{1+z}, \text{ and} \quad (2.6a)$$

$$\frac{c}{H(z) r_d} = \frac{c}{H_0 r_d} \frac{1}{h(z)}, \text{ where} \quad (2.6b)$$

$$\frac{H_0 r_d}{c} = \frac{1}{\sqrt{3}} \int_0^{\frac{1}{1+z_d}} \frac{da}{a^2 h(a) \sqrt{1 + \frac{3\omega_b}{4\omega_\gamma} a}} \quad (2.6c)$$

and r_d is the sound horizon at the drag epoch z_d . $H_0 r_d$ is thus an interesting parameter combining early- and late-time physics, which may play an important role in the H_0 tension [31–34].

3 Data

In this analysis, we used simulated 3-year LSST¹ SNIa data and the BAO forecast for DESI from [35] to constrain cosmology.

3.1 Fiducial Models

To show the potential of our model-independent approach, we simulate data for four different fiducial cosmologies. All fiducial cosmologies share the same $(\Omega_{m,0}, h) = (0.315, 0.7)$, which is the cosmology used in [36].

- Flat- Λ : a flat- Λ CDM universe, with a constant equation of state $w = -1$.
- k - Λ : a curved Λ CDM universe, with $\Omega_{k,0} = 0.1$. While such a large curvature is consistent with Pantheon+ or DESI DR1 data, it is excluded by Planck 2018 data. However, it is nonetheless interesting to see the effect of curvature and to apply our curvature test to a curved universe.
- Flat-PEDE: a flat universe with dynamical dark energy. We chose the phenomenologically emergent dark energy (PEDE) model [37], which has no extra degree of freedom relative to Λ CDM. The dark energy density evolves as

$$f_{\text{PEDE}}(z) = 1 - \tanh(\log_{10}(1+z)) \quad (3.1a)$$

and the equation of state

$$w_{\text{PEDE}}(z) = \frac{1}{3 \ln 10} (1 + \tanh[\log_{10}(1+z)]) - 1 \quad (3.1b)$$

- k -PEDE: a curved universe with $\Omega_{k,0} = 0.1$ and PEDE.

¹www.lsst.org

Fiducial Cosmology	$\Omega_{k,0}$	w	$\chi^2_{\Lambda\text{CDM}}$	$\Delta\chi^2_{\text{fid}}$
ΛCDM	0	-1	7.48	1.27
$k\text{-}\Lambda\text{CDM}$	0.1	-1	11.68	-2.93
PEDE	0	Eq. (3.1b)	8.21	0.54
$k\text{-PEDE}$	0.1	Eq. (3.1b)	7.55	1.20

Table 1: Fiducial cosmologies used in this work. The fourth column shows the ΛCDM χ^2_{fid} to the data, used as a reference throughout this work, and the last column shows the $\Delta\chi^2$ of the fiducial model with respect to the best-fit ΛCDM .

We note that the SNIa mock data and covariance matrix were initially generated for the flat ΛCDM case. We extracted the noise $\mu - \mu_{\text{fid}}$ and applied it to the other three fiducial cosmologies. Although for a proper forecast, one should apply the pipeline from [36] to the other three fiducial cosmologies, we assume here that the resulting noise and covariance should be affected minimally by the change of fiducial cosmology. On the other hand, the mock BAO data are all generated with a Gaussian white noise as detailed in Section 3.3.

Table 1 summarizes our four fiducial cosmologies.

3.2 LSST SNIa Simulations

3.2.1 The Rubin Observatory Legacy Survey of Space and Time (LSST)

The forthcoming LSST survey, scheduled to commence in 2025, represents the most comprehensive optical survey planned to date, marking a significant milestone for its generation. This survey will run for a decade and will extensively explore the southern hemisphere’s sky through a large, ground-based, wide-field observatory utilising six optical passband filters. This combination is designed to achieve an unparalleled balance of depth, coverage area, and observational frequency. Over the course of the survey, the LSST is expected to catalogue millions of supernovae [38]. Operating from the Vera C. Rubin Observatory, the Simonyi Survey Telescope features an 8.4 m mirror (with an effective aperture of 6.7 m) and is equipped with a state-of-the-art 3200-megapixel camera, providing a 9.6 deg² field of view. Approximately 90% of the telescope’s time will be dedicated to a deep-wide-fast survey mode, systematically covering an area of 18,000 square degrees roughly 800 times across all bands over a decade, resulting in a co-added map with a depth of $r - 27.5$ (called as the Wide Fast Deep (WFD) observing strategy in the LSST). This extensive data collection is projected to amass around 32 trillion observations of 20 billion galaxies and an equivalent number of stars, primarily supporting the survey’s main scientific objectives [38]. The remaining 10% of the time will be reserved for specific initiatives, such as the Very Deep and Very Fast time-domain surveys,² which are still in the planning stages.

3.2.2 Mock Data Generation

This study employs simulated SNIa data to examine dark energy results from the forthcoming LSST observations, as detailed in [36]. The supernova data are generated through the LSST Dark Energy Science Collaboration (DESC) Time Domain (TD) pipeline and the **SNANA** software [39]. In this analysis, our SN data refers to using the corresponding Hubble diagram, and the covariance matrix provided by [36]. The Hubble diagram consists of the redshift (z)

²Deep Drilling Fields (DDF)

of measurements, the corresponding luminosity distance (D_L), and their statistical plus systematic errors combined ($\sigma(D_L)$). The procedure encompasses four primary stages, depicted in Figure 4 of [36].

The simulations utilise the flat Λ CDM model from § 3.1. In particular, the Hubble constant, H_0 , is set at $70.0 \text{ km s}^{-1} \text{ Mpc}^{-1}$, aligned with the SALT2 model training. The SALT2 light curve model is employed to derive observer frame magnitudes. The simulation noise is calculated using the following equation:

$$\sigma_{\text{SIM}}^2 = [F^2 + (A \cdot b)^2 + (F \cdot \sigma_{\text{ZPT}})^2 + \sigma_0 \cdot 10^{0.4 \cdot ZPT_{\text{pe}}} + \sigma_{\text{host}}^2] S_{\text{SNR}}^2. \quad (3.2)$$

where F represents the simulated flux in photoelectrons, A denotes the noise equivalent area, given by $A = [2\pi \int \text{PSF}^2(r, \theta) r dr]^{-1}$, with PSF standing for the Point Spread Function, and b represents the background per unit area (inclusive of sky, CCD readouts, and dark current). The scale factor S_{SNR} is empirically determined based on the signal-to-noise ratio. The terms represented by σ denote uncertainties related to zero point, flux calibration, and the underlying host galaxy, empirically fitted to match simulated uncertainties with those derived from the survey designs.

The LSST TD pipeline involves SN brightness standardisation via a Light Curve (LC) fit stage, simulations for bias correction, and a BEAMS with Bias Corrections (BBC) stage for Hubble diagram production. This pipeline yields a redshift-binned Hubble diagram and its associated covariance matrix, which are the data products employed for cosmological fitting.

The SNIa dataset utilised comprises both spectroscopically (z_{spec}) and photometrically (z_{phot}) identified SNIa candidates. Based on PLAsTiCC [40], the “ z_{spec} ” sample includes two sets of events with spectroscopic redshifts featuring an accuracy of $\sigma_z \sim 10^{-5}$. The first subset consists of spectroscopically confirmed events with accurate redshift predictions by the 4MOST spectrograph [41], under construction by the European Southern Observatory and expected to be operational in 2024, situated at a latitude similar to that of the Rubin Observatory in Chile. The second subset includes photometrically identified events with accurate host galaxy redshifts determined by 4MOST, with this subset being approximately 60% larger than the first. For the photometric sample, host galaxy photometric redshifts were employed as priors (adapted from [42]). The photometric redshift and rms uncertainty derive from [43]. The entire simulation was rerun based on the PLAsTiCC DDF data³. Additional low redshift spectroscopic data was sourced from the DC2 analysis, simulated with WFD cadence. [36] restricted simulations to SNIa, omitting contamination (*e.g.* core collapse, peculiar SNe, *etc.*). The covariance matrix corresponds to the combined statistical and systematic errors, where the latter encompasses all individual systematics, detailed in Table 3 of [36]. The Hubble diagram is segmented into 14 redshift bins, containing a total of 5809 SNIa candidates, both spectroscopic and photometric.

It is noteworthy that [36] introduce a dataset with characteristics akin to those projected in the LSST science roadmap for 1 and 10 years of SNIa cosmology analysis, as described by [44]. However, there are significant differences. While the analysis by [44] relies solely on SNIa with spectroscopically confirmed host redshifts, [36] broadens the scope by including a comprehensive end-to-end analysis that incorporates both spectroscopic and photometric redshifts of host galaxies. In the forthcoming LSST era, it is anticipated that the volume of photometrically observed Type Ia supernovae will vastly outnumber the spectroscopic candidates. The methodology presented in [36] therefore enables the use of these photometric

³The LSST utilises different observing strategies, namely the deep field and the wide field, termed the DDF (Deep Drilling Field) and the WFD (Wide Fast Deep), respectively.

candidates in the cosmology analysis and hence in construction of a denser Hubble diagram with higher redshift reaches. As a result, this presents a critical opportunity to leverage photometric supernovae in cosmological analyses, and potentially amplifying the dark energy constraints significantly.

We would also like to mention that the SN analysis done using the LSST Time-Domain pipeline used a Gaussian SN likelihood, but the method presented in our analysis here, can as well incorporate asymmetric and non-Gaussian errors. Therefore our methodology will still apply, even if we had a different covariance matrix and likelihood for our data (including non-gaussian likelihoods). The fourth column of Table 1 shows the Λ CDM χ^2 to the SNIa data for each fiducial cosmology. As expected, the flat- Λ cosmology has the lowest $\chi^2_{\Lambda\text{CDM}}$. The last column shows $\Delta\chi^2 = \chi^2_{\text{fid}} - \chi^2_{\Lambda\text{CDM}}$, the difference between the χ^2 of the fiducial cosmology to that of the Λ CDM best-fit. It is worth noting that, since we use the same noise for all cosmologies, χ^2_{fid} is the same for all four cosmologies, in this case 8.75. Therefore, $\Delta\chi^2_{\text{fid}}$ is larger for the flat- Λ cosmology.

3.3 Mock BAO data from DESI 5-year

The Dark Energy Spectroscopic Instrument (DESI) is a stage-IV experiment aiming to constrain dark energy by mapping the Universe in three dimensions [6]. In particular, DESI is measuring the BAO, a probe of the expansion history from large-scale structures.

We generated DESI 5-year mock BAO, assuming a Gaussian white noise where the errors on d_A and H are taken from [35], assuming a correlation coefficient of 0.4 between d_A and H , and then propagated to errors on d_A and d_H via the usual error propagation formula for correlated variables.

We also assume $H_0 = 70 \text{ km s}^{-1} \text{ Mpc}^{-1}$, and $r_d^{\text{fid}} = 144.0533 \text{ Mpc}$, leading to a fiducial value of $H_0 r_d = 10\,083.731 \text{ km s}^{-1} = c/29.73$). This fiducial value of r_d can be obtained for the Λ CDM fiducial cosmology with $\omega_b = 0.02237$. While the value of r_d would be calculated to be different for the other three fiducial cosmologies, we chose fix the value of r_d to the same value for the four fiducial cosmologies. While such a choice of H_0 is not currently favored by CMB experiments, the exact choice of cosmological parameters is not important for the purpose of this study since we are focusing on model independent reconstructions and so our results do not depend on different fiducial models.

4 Method

Several litmus tests have been put forward to test various aspects of the Λ CDM model. In particular, the \mathcal{O}_k diagnostic [31, 45, 46] is defined as

$$\mathcal{O}_k(z) = \frac{\Theta^2(z) - 1}{\mathcal{D}^2(z)}, \quad (4.1a)$$

where

$$\Theta(z) = h(z)\mathcal{D}'(z), \quad (4.1b)$$

where $'$ denotes the derivative with respect to redshift. In an FLRW universe, $\mathcal{O}_k(z) \equiv \Omega_{k,0}$, and $\Theta(z) = \sqrt{1 + \Omega_{k,0}\mathcal{D}^2}$, and in a flat-FLRW universe, $\Theta(z) \equiv 1$. It is important to realize that these equalities only assume the FLRW metric, and in particular, are independent of the dark energy evolution.

The $\mathcal{O}m$ diagnostic, introduced by [47], is defined as

$$\mathcal{O}m(z) = \frac{h^2(z) - 1}{(1+z)^3 - 1} = \Omega_{m,0} \quad (4.2)$$

in a flat- Λ CDM universe. These two diagnostics are litmus tests respectively of the FLRW metric (and its curvature) and of the flat- Λ CDM model. Departure from $\mathcal{O}m = \text{constant}$, or from $\mathcal{O}_k = \text{constant}$ are signs of departure from flat- Λ CDM and FLRW respectively.

Another widely used quantity is the deceleration parameter

$$q = -\frac{1}{H} \frac{\ddot{a}}{a} = -(1+z) \frac{h'}{h} - 1, \quad (4.3)$$

where $\dot{}$ denotes the derivative with respect to time t . $q > 0$ indicate a decelerating Universe, while $q < 0$ for an accelerating universe.

4.1 Curvature test

The transverse and radial BAO modes respectively give us $d_A/r_d = d_M/((1+z)r_d)$ and $d_H/r_d = c/(Hr_d)$, while the supernovae provide \mathcal{D} and \mathcal{D}' , which are independent of both H_0 and r_d . Intuitively, the SNIa constrain (the log of) \mathcal{D} , and we can obtain \mathcal{D}' by calculating the smooth derivative of \mathcal{D} (see Section 4.2). We can therefore combine these two measurements to estimate $H_0 r_d$ in two independent ways:

$$\frac{c}{H_0 r_d} = \frac{1}{\mathcal{D}(z)} \frac{d_M(z)}{r_d}, \text{ and} \quad (4.4a)$$

$$\frac{c}{H_0 r_d} = h(z) \frac{c}{H r_d} = \frac{1}{\mathcal{D}'(z)} \frac{d_H(z)}{r_d}, \quad (4.4b)$$

where the last equality in eq. (4.4b) holds only for a flat-FLRW universe. Therefore, we can combine the BAO observables with \mathcal{D} and \mathcal{D}' measured by SNIa to constrain $H_0 r_d$. One way to do this is to reconstruct a smooth comoving distance $\mathcal{D}(z)$, its derivative $\mathcal{D}'(z)$, and expansion history $h(z)$ from SNIa at any arbitrary redshift z , and evaluate those curves at the BAO redshifts z_{BAO} . To do the reconstructions, we apply the iterative smoothing method to simulated LSST SNIa as described in Section 4.2. We then simply divide the central value of the BAO measurements d_M/r_d and d_H/r_d by the value of the reconstructed \mathcal{D} and \mathcal{D}' evaluated at the BAO redshifts and then propagate the BAO error.

We can then calculate

$$\Theta(z) = \frac{H(z)r_d}{H_0 r_d} \mathcal{D}'(z) = \frac{d_M(z)/r_d}{d_H(z)/r_d} \frac{\mathcal{D}'(z)}{\mathcal{D}(z)} \quad (4.5)$$

and \mathcal{O}_k only with the BAO and the smooth reconstructions from the SNIa data. Similarly to $H_0 r_d$, we evaluate $\Theta(z)$ by multiplying the central values of the BAO data (d_H/r_d and d_M/r_d) with the smooth functions reconstructed from the SNIa (\mathcal{D}'/\mathcal{D}), evaluated at the BAO redshifts z_{BAO} , and propagating the error by taking the covariance between d_M and d_H as detailed in Appendix B.

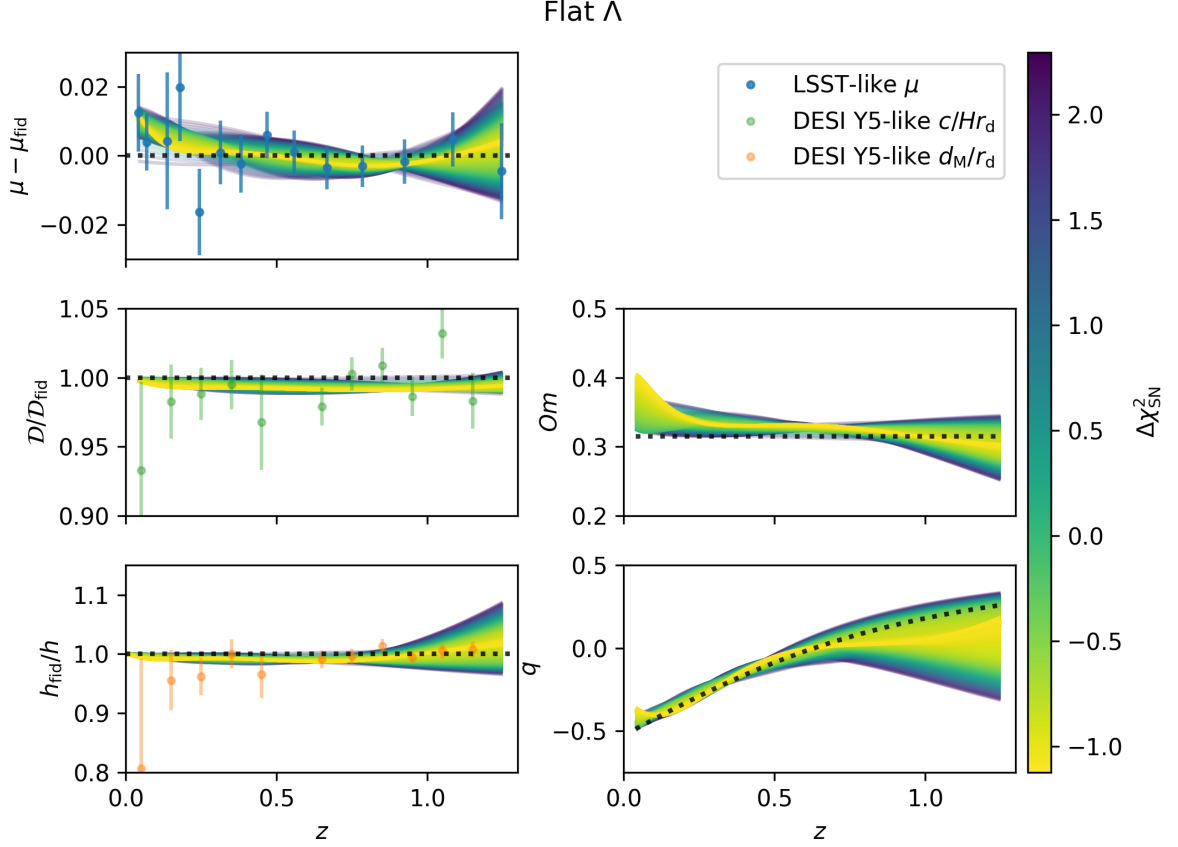


Figure 1: Results of the SNIa smoothing colour-coded by $\Delta\chi^2_{\text{SN},n} = \chi^2_{\text{SN},n} - \chi^2_{\text{SN},\Lambda\text{CDM}}$ for the flat- Λ CDM fiducial cosmology. The top-left panel shows the smooth residuals. The middle-left panel shows $\mathcal{D}/\mathcal{D}_{\text{fid}}$, the bottom-left panel shows h_{fid}/h , the middle-right panel shows $\mathcal{O}m$, and the bottom-right panel q . The middle- and bottom-left panels also show the DESI-like BAO mock data normalized by the fiducial cosmology.

4.2 Iterative Smoothing

We used the iterative smoothing method to reconstruct the distance-redshift relation from SNIa [32, 48, 49]. The strength of this method is that we make no assumption regarding the evolution of dark energy.

Starting with some initial guess $\hat{\mu}_0$, we iteratively calculate the reconstructed $\hat{\mu}_{n+1}$ at iteration $n + 1$ with the inverse covariance matrix of the SNIa data $\mathbf{C}_{\text{SN}}^{-1}$:

$$\hat{\mu}_{n+1}(z) = \hat{\mu}_n(z) + \frac{\delta\boldsymbol{\mu}_n^\top \cdot \mathbf{C}_{\text{SN}}^{-1} \cdot \mathbf{W}(z)}{\mathbb{1}^\top \cdot \mathbf{C}_{\text{SN}}^{-1} \cdot \mathbf{W}(z)}, \quad (4.6a)$$

where

$$\mathbf{W}_i(z) = \exp\left(-\frac{\ln^2\left(\frac{1+z}{1+z_i}\right)}{2\Delta^2}\right) \quad (4.6b)$$

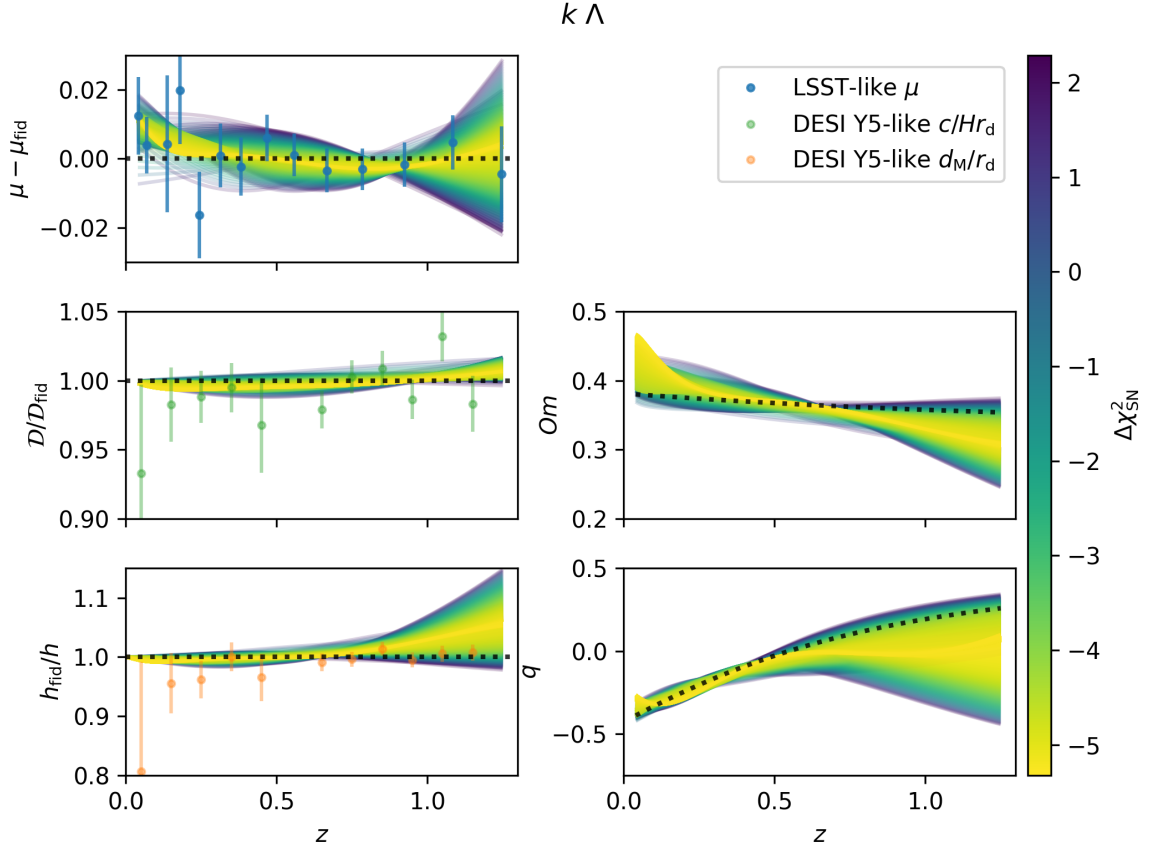


Figure 2: Same as Fig. 1, fiducial model: k - Λ CDM. Note that in the bottom-left panel, the BAO data are h_{fid}/h , but the smooth SNIa reconstructions show $\mathcal{D}'/\mathcal{D}'_{\text{fid}}$.

is the smoothing kernel,

$$\mathbb{1} = (1, \dots, 1)^\top \quad (4.6c)$$

is a column vector,

$$\delta\mu_n|_i = \mu_i - \hat{\mu}_n(z_i). \quad (4.6d)$$

The smoothing width is set to $\Delta = 0.3$ following previous analyses in [31, 32, 48–53]. $W(z)$ can be understood as a Gaussian smoothing kernel of the variable $u = \ln(1+z)$, and the denominator as a normalization factor.

We define the χ^2 value of the reconstruction $\hat{\mu}_n(z)$ at iteration n as

$$\chi_{\text{SN},n}^2 = \delta\mu_n^\top \cdot \mathbf{C}_{\text{SN}}^{-1} \cdot \delta\mu_n. \quad (4.7)$$

The results converge towards the solution preferred by the data, independently from the choice of the initial condition [31, 32, 48, 49]. Therefore, starting from different initial conditions, the results of the iterative smoothing method will approach this solution by different paths. More precisely, we start from the best-fit k - Λ CDM, flat Λ CDM, and flat Λ CDM with fixed $\Omega_{\text{m},0} = \{0, 0.1, \dots, 1\}$. We collect all reconstructions with $\Delta\chi_{\text{SN},n}^2 = \chi_{\text{SN},n}^2 - \chi_{\text{SN,LCDM}}^2 <$

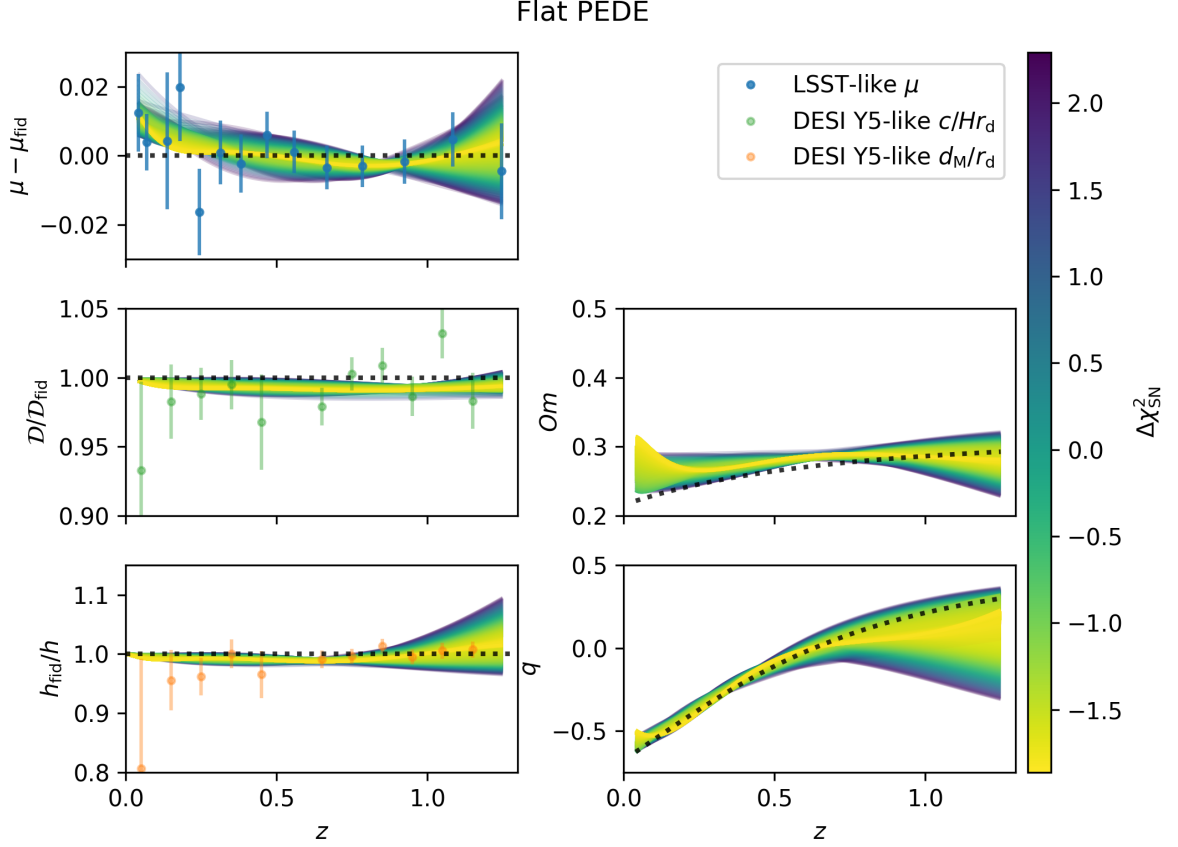


Figure 3: Same as Fig. 1, fiducial model: Flat-PEDE

2.3 relative to the best-fit Λ CDM. These reconstructions then make up a non-exhaustive set of plausible distances and expansion histories.

We also obtained the smoothed first and second derivatives of $\hat{\mu}$ as described in Appendix A. The initial guess for the derivative of the distance modulus is

$$\frac{d}{d\ln(1+z)}\hat{\mu}(z) = \frac{5}{\ln 10} \left[1 + \frac{1+z}{h\mathcal{D}} \sqrt{1 + \Omega_{k,0}\mathcal{D}^2} \right], \quad (4.8)$$

$$\frac{d^2}{d\ln(1+z)^2}\hat{\mu}(z) = \frac{5}{\ln 10} (1+z) \left[\frac{\mathcal{D}'}{\mathcal{D}} \left(1 - (1+z) \frac{\mathcal{D}'}{\mathcal{D}} \right) + (1+z) \frac{\mathcal{D}''}{\mathcal{D}} \right], \quad (4.9)$$

where $'$ denotes d/dz . The derivatives of μ are directly obtained during the smoothing process of the supernovae. The formalism of the smooth derivative is described in the appendix.

From $\hat{\mu}$, $\hat{\mu}'$, and $\hat{\mu}''$, we can reconstruct

$$\mathcal{D}(z) = \frac{H_0}{c} 10^{\frac{\mu}{5}-5} \quad (4.10)$$

$$\mathcal{D}'(z) = \left[\frac{\ln 10}{5} \frac{d\mu}{d\ln(1+z)} - 1 \right] \frac{\mathcal{D}(z)}{1+z}, \text{ and} \quad (4.11)$$

$$\mathcal{D}''(z) = -\frac{\mathcal{D}'}{1+z} + \left[\frac{\ln 10}{5} \frac{d^2\mu}{d(\ln(1+z))^2} \mathcal{D} \right] + \left[\frac{\ln 10}{5} \frac{d\mu}{d\ln(1+z)} - 1 \right] \frac{\mathcal{D}'}{1+z} \quad (4.12)$$

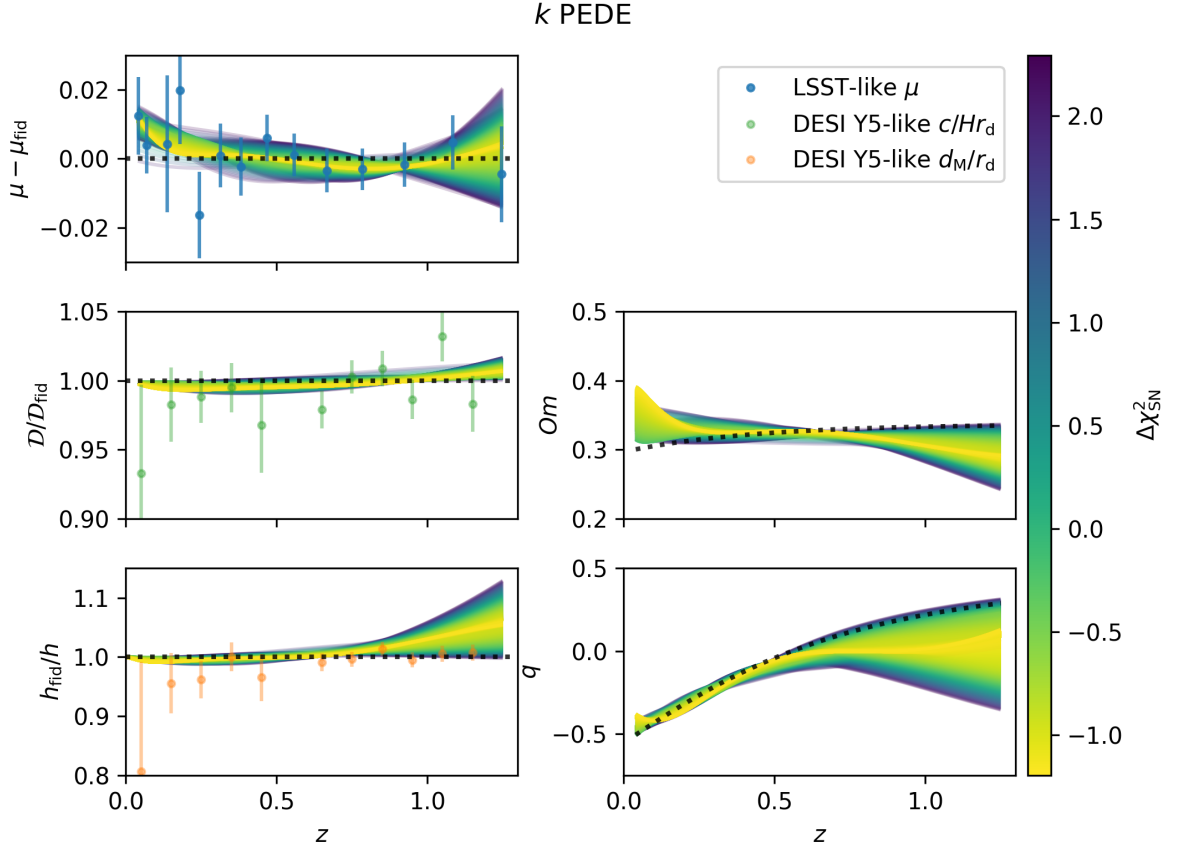


Figure 4: Same as Fig. 1, fiducial model: k -PEDE

In practice, $\hat{\mu}$ is reconstructed to an additive constant, and one has to normalize \mathcal{D} , \mathcal{D}' , and \mathcal{D}'' so that $\mathcal{D}'(z=0) = 1$.

From these relations, we can obtain h , h' , \mathcal{D}' via

$$\mathcal{D}' = \frac{\mathcal{D}}{1+z} \left(\frac{\ln 10}{5} \frac{d\mu}{d\ln(1+z)} - 1 \right) \quad (4.13)$$

$$h = \frac{\sqrt{1 + \Omega_{k,0} \mathcal{D}^2}}{\mathcal{D}'} \quad (4.14)$$

and

$$h' = \frac{h\mathcal{D}}{\mathcal{D}'} \left[\frac{\Omega_{k,0}}{h^2} - \frac{\mathcal{D}''}{\mathcal{D}} \right]. \quad (4.15)$$

It is worth noting that, while we can obtain \mathcal{D}' and \mathcal{D}'' from the smoothing of the supernovae directly, to obtain h and h' , one needs to know $\Omega_{k,0}$. Therefore, wrongly assuming flatness will imply an error when inferring $h(z)$, $h'(z)$, and $q(z)$. This is just a restatement of the \mathcal{O}_k test. In addition, it is worth noticing that, while BAO provide both separate (but correlated) measurement of d_M/r_d and d_H/r_d , \mathcal{D} , \mathcal{D}' and \mathcal{D}'' are obtained from the same measurements.

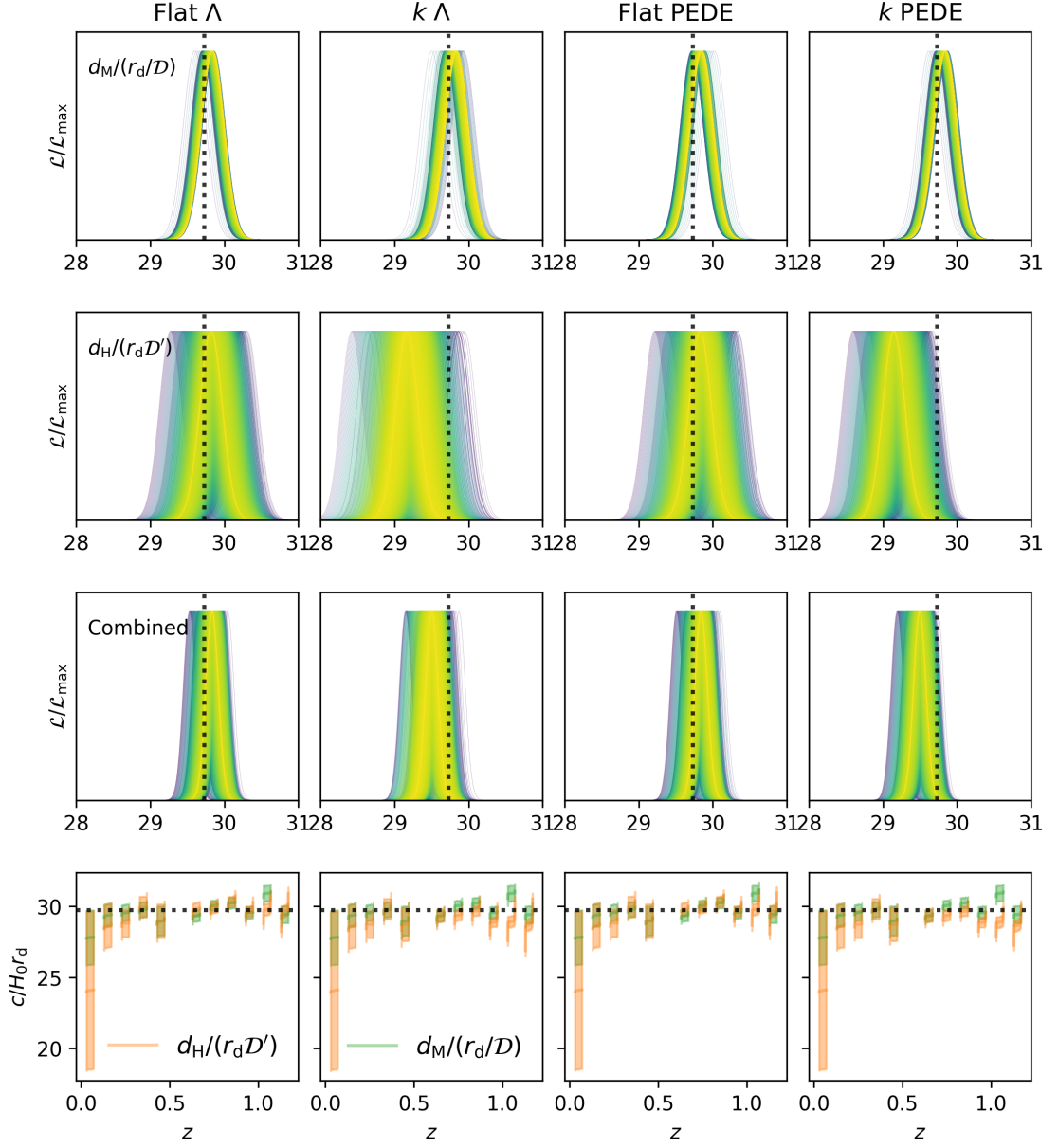


Figure 5: The bottom row shows our estimations of $c/H_0 r_d$ for our two methods (Eqs. (4.4a) and (4.4b)) at the BAO data points for the four fiducial cosmologies. The black dotted line is the fiducial value. The central line is the collection of central values of $c/H_0 r_d$ for each reconstruction, and the coloured band is the one-sigma error from the BAO around the central value. The top rows show the likelihood for estimate (4.4a) at fixed iteration, and the second row for estimate (4.4b), and the third row shows the combination of both, taking into account the correlation. The colour bars of the top three rows are the same as that of the corresponding smooth figures (1 to 4).

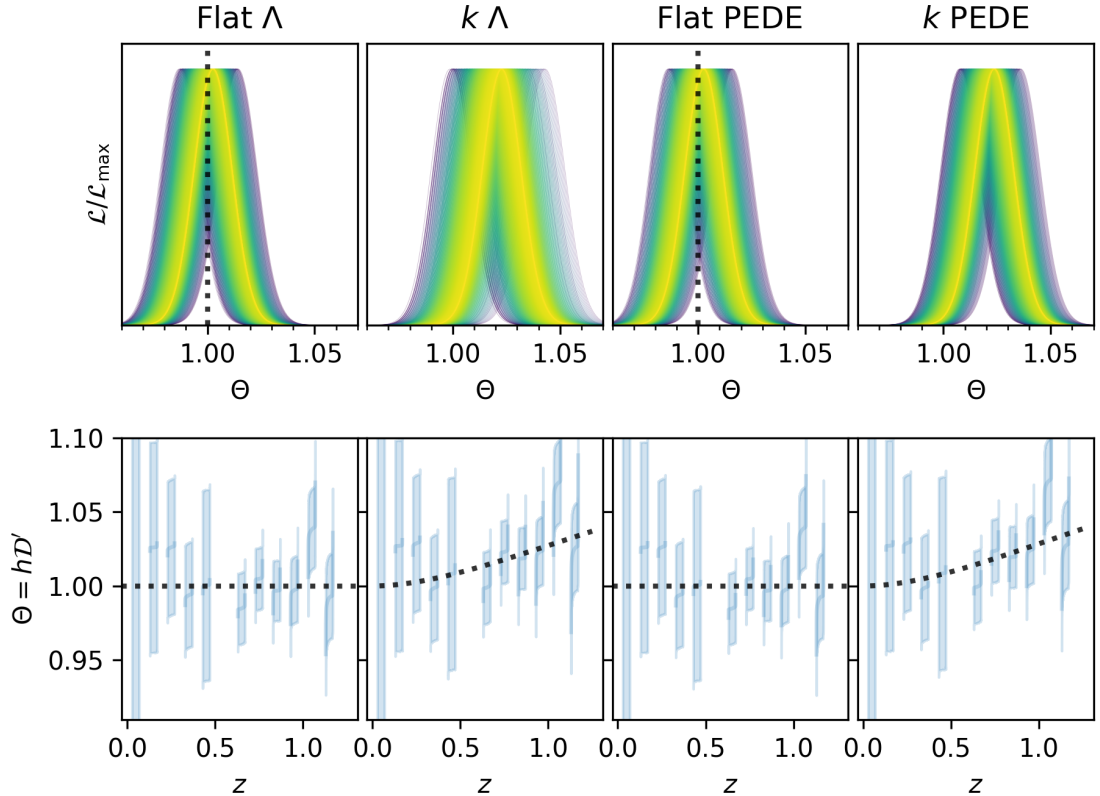


Figure 6: Curvature parameter: Θ . The bottom row shows $\Theta = h\mathcal{D}'$ for our four fiducial cosmologies. Like in Fig. 5, the central value is obtained by combining the BAO with each iteration of the smooth SN reconstructions, and the error-band from the 1σ errors from the BAO. The top row shows the likelihood of Θ for each smooth reconstruction. We note that in the second and fourth panels of the top row, there is no true value for Θ since $\Theta(z) = \sqrt{1 + \Omega_{k,0}\mathcal{D}^2}$ varies with redshift.

5 Results

5.1 Supernova Smoothing

Fig. 1 shows the results of the smoothing for the flat- Λ CDM fiducial model. Each line is an iteration of the smoothing color-coded by its $\Delta\chi^2$ with respect to the best-fit Λ CDM model. The top-left panel shows the reconstructed distance moduli with the mock SNIa data. The middle- and bottom-left panels show the comoving distance $\mathcal{D}(z)/\mathcal{D}_{\text{fid}}(z)$ and the inverse of the expansion history $h_{\text{fid}}(z)/h(z)$ normalized to the fiducial values. Again, the colored lines come from the smoothing of the SNIa, while the data points with error-bars come from the BAO. The middle- and bottom-right panels show $\mathcal{O}m$ and the deceleration parameter q . We are able to reconstruct the fiducial quantities. We report the $\Delta\chi^2_{\text{fid}} = \chi^2_{\text{fid}} - \chi^2_{\Lambda\text{CDM}}$ in the last column of Table 1.

Figs. 2, 3, 4 show the same results for the $k\Lambda$ CDM, flat-PEDE, and k -PEDE fiducial models. In all cases, we are able to reconstruct the $\mathcal{O}m$ and q parameters. However, it is

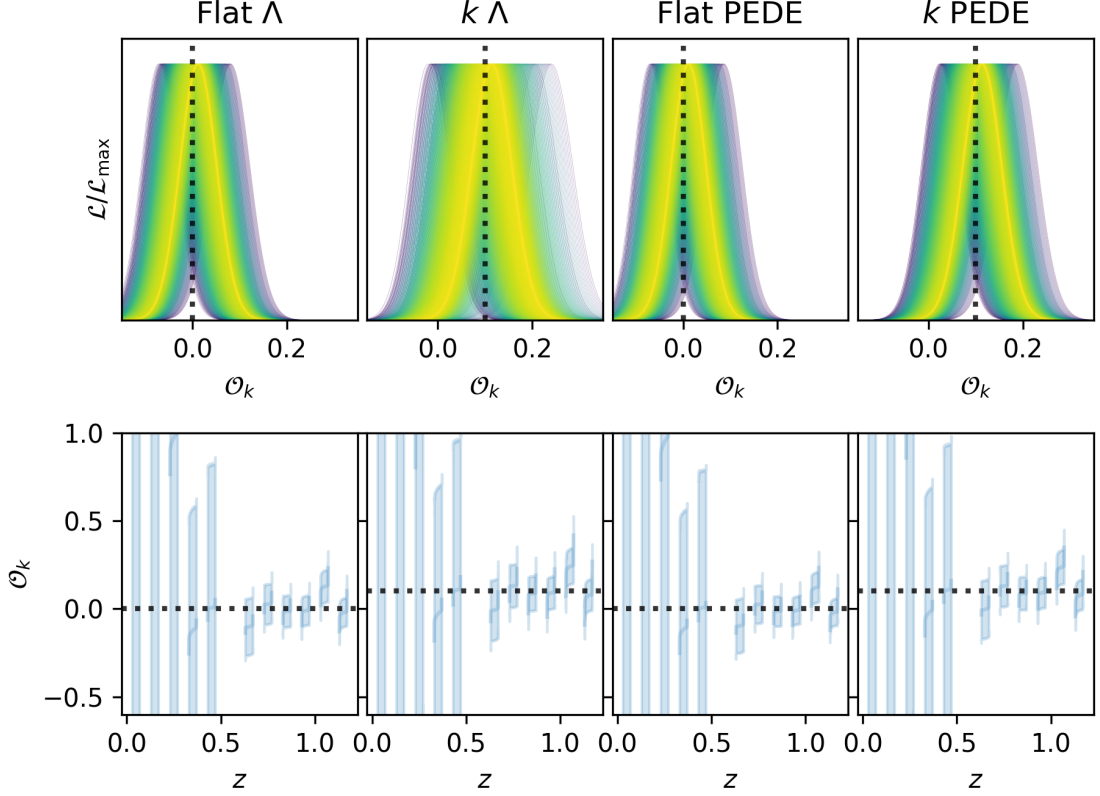


Figure 7: Curvature test: the \mathcal{O}_k diagnostic. Same legend as Figs. 6. The black dotted lines in the bottom row show the fiducial values of $\Omega_{k,0}$ in all three panels, $\Omega_{k,0} = 0$ for the left and right, and $\Omega_{k,0} = 0.1$ for the center. It is worth noting that in the $\Omega_{k,0} = 0.1$ case, the \mathcal{O}_k diagnostic recovers the non-zero fiducial value of $\Omega_{k,0}$.

interesting to look closely at the two non-flat cases. Since the assumption of flatness that goes into eq. (2.3) is not true in this case, calculating \mathcal{D}' does not provide h (see eq. (4.14)). This in turn will bias our inference of \mathcal{O}_m and q as well as the curvature test. At high-enough redshifts $z \geq 1$, the deviation between \mathcal{D}' and $1/h$ (i.e., $\sqrt{1 + \Omega_{k,0}\mathcal{D}^2}$) becomes important. This deviation between the h_{fid}/h data from the BAO and the \mathcal{D}'/\mathcal{D} reconstructions from the SNIa are the litmus test for flatness, or signal for curvature that we are looking for. Interestingly, the reconstructions are still consistent with the fiducial q .

5.2 $H_0 r_d$

The bottom row of Fig. 5 shows our two estimations of $c/H_0 r_d$ from eqs (4.4a) and (4.4b) for each fiducial model. At each BAO data point, we plot the central value and the $\pm 1\sigma$ band for each reconstruction n with $\Delta\chi_{\text{SN},n}^2 = \chi_{\text{SN},n}^2 - \chi_{\text{SN},\Lambda\text{CDM}}^2 < 2.3$. It is worth stressing here that at every BAO point, we have N_{rec} estimations of $c/H_0 r_d$, corresponding to N_{rec} reconstructions of the distance-redshift relations from the SNIa (combined with the mock BAO data point). Each of these estimates also has an associated error bar, shown as an error band on the figure. At each redshift point, the reconstructed $c/H_0 r_d$ are re-sorted by

increasing central value for aesthetic reasons. The fiducial value $c/H_0 r_d^{\text{fid}} = 29.73$ is shown as a dashed line. For the four fiducial cosmologies, the estimations from eq. (4.4a) are consistent with $H_0 r_d^{\text{fid}}$.

Rows 1 to 3 show the (normalized) likelihood for iteration n

$$\mathcal{L}_{n,i}(x) \propto \exp\left(-\frac{\chi_n^2}{2}\right), \text{ where} \quad (5.1a)$$

$$\chi_n^2 = -\frac{1}{2}(x\mathbb{1} - \mathbf{X}_i)^\top \cdot \mathbf{C}_i^{-1} \cdot (x\mathbb{1} - \mathbf{X}_i), \quad (5.1b)$$

$$\mathbf{X}_1^\top = \left(\frac{1}{\mathcal{D}(z_1)} \frac{d_M(z_1)}{r_d}, \dots, \frac{1}{\mathcal{D}(z_N)} \frac{d_M(z_N)}{r_d}\right), \quad (5.1c)$$

$$\mathbf{X}_2^\top = \left(\frac{1}{\mathcal{D}'(z_1)} \frac{d_H(z_1)}{r_d}, \dots, \frac{1}{\mathcal{D}'(z_N)} \frac{d_H(z_N)}{r_d}\right), \quad (5.1d)$$

$$\mathbf{X}_3 = \begin{pmatrix} \mathbf{X}_1 \\ \mathbf{X}_2 \end{pmatrix} \quad (5.1e)$$

are the data vectors, and $N = 11$ is the number of BAO data points. The error propagation, including the covariance between the two BAO modes, is detailed in Appendix B. In the case of eq. (4.4a) (row 1), the three fiducial cosmologies yield similar reconstructions, regardless of the curvature and DE. This is to be expected, since both distances from the SNIa and BAO should agree regardless of the curvature. It is worth paying attention to the k - Λ and k -PEDE cases (second and fourth columns). While estimator (4.4a) (row 1) is totally consistent with the fiducial value, eq. (4.4b) (row 2) is centred around 28 to 29, and most of the reconstructions are over 2σ away from the fiducial value, showing an inconsistency between the two estimators. This comes from the fact that while the radial mode of the BAO provides us with $1/h$, the SNIa provide us with \mathcal{D}' , which do not coincide in a non-flat FLRW universe, as seen above. Indeed, we can see in the bottom row that the values of $d_H/(r_d \mathcal{D}')$ diverge from the fiducial values at high redshift, reflecting equation (4.14). For each quantity A , we report the minimal and maximal values of the precision σ_A and the spread $\Delta A = (A - A_{\text{fid}})$ taken over all reconstructions in Table 2. Namely, for a given reconstruction n , we obtain the likelihood in the top three panels, and obtain the corresponding precision and spread. We then report the minimal and maximal value over the whole reconstructions. In the case of X_i (eqs. (5.1c) to (5.1e)), we normalize the result by the fiducial value. The third row shows a greater precision by combining the two estimators despite the correlation between the radial and transverse BAO modes.

5.3 Curvature Test

The bottom panel of Fig. 6 shows our estimate of $\Theta(z) = h\mathcal{D}' = \sqrt{1 + \Omega_{k,0}\mathcal{D}^2}$ for the three cosmologies. The top panel shows the normalized likelihood of $\Theta(z)$ over z for a given iteration of the smoothing, colour-coded by $\Delta\chi^2$ of the SNIa reconstruction. As expected, for the Flat- Λ (left) and PEDE (right) cases, our estimates are consistent with $\Theta = 1$. The interesting cases are the k - Λ and k -PEDE cases (second and fourth columns). We can see in the bottom panel a trend of $\Theta(z)$ deviating from 1 as z increases. Similarly, in the top panel, the likelihoods peak at higher values than in the other two cases, and only marginally consistent with $\Theta = 1$.

Fig. 7 shows similar plots for the \mathcal{O}_k parameter. Similarly to Θ , the Flat- Λ and PEDE case are perfectly consistent with flatness ($\Omega_{k,0} = 0$), while the $\Omega_{k,0} = 0.1$ case is only

Quantity	flat- Λ	k - Λ	PEDE	k -PEDE
$\sigma_{X_1}/X_{\text{fid}}$	0.52%	0.52%	0.52 – 0.53%	0.52%
$\Delta X_1/X_{\text{fid}}$	-0.44% – 0.44%	-0.77% – 0.68%	-0.05% – 0.98%	-0.37% – 0.49%
$\sigma_{X_2}/X_{\text{fid}}$	0.50 – 0.52%	0.49 – 0.51%	0.50 – 0.52%	0.49 – 0.51%
$\Delta X_2/X_{\text{fid}}$	-1.55% – 1.94%	-4.40% – 0.72%	-1.74% – 2.04%	-3.82% – -0.18%
$\sigma_{X_3}/X_{\text{fid}}$	0.28 – 0.29 %	0.28%	0.28 – 0.29%	0.28%
$\Delta X_3/X_{\text{fid}}$	-0.68% – 1.06%	-1.96% – 0.47%	-0.75% – 1.24%	-1.82% – 0.02%
$\sigma_{\mathcal{O}_k}$	0.037 – 0.040	0.040 – 0.045	0.035 – 0.038	0.039 – 0.042
$\Delta \mathcal{O}_k$	0.004 – 0.015	-0.095 – -0.031	0.004 – 0.016	-0.095 – -0.055
σ_{Θ}	0.009	0.009	0.009	0.009
$\Delta \Theta$	-0.026 – 0.029	—	-0.0277 – 0.0332	—

Table 2: Table of precision and spread for our four fiducial cosmologies. The reported values are the minimum and the maximum values of the 1σ CL of the likelihoods in Figs. 5 to 7 over all reconstructions. The spread of quantity A , noted as ΔA is defined as the difference between the peak of the likelihood and the fiducial value. For simplicity, we note $X = c/H_0 r_d$, and the indices refer to the different estimators (see eqs. (5.1c) to (5.1e)). The precisions for our three estimates of $X = c/H_0 r_d$ are relative to the true value, while the precisions and spreads in \mathcal{O}_k and Θ are absolute. We note that in the non-flat cases (k - Λ and k -PEDE), there is no *fiducial* value for Θ since Θ evolves with redshift, so we do not report the spread.

marginally consistent with $\Omega_{k,0} = 0$ and perfectly consistent with $\Omega_{k,0} = 0.1$, showing the constraining power of this test.

In the bottom panels of both figures, at $z \gtrsim 0.5$, the error bars are very small and the reconstructions are perfectly consistent with the fiducial cosmology in all three cases. At low redshift, the large error bars do not constrain Θ or $\Omega_{k,0}$.

In order to assess the power and significance of the test, we perform a hypothesis test. One must bear in mind that the problem is not symmetric here: the null hypothesis H_0 to test is “ $\Omega_{k,0} = 0$ ”. For the two flat models, we are interested in type I errors: what is p_I , the probability of wrongly rejecting flatness? For the two non-flat models, the question is “What is the probability of failing to reject flatness?”, i.e., type II errors, with probability p_{II} .

To assess these, we resimulate 1000 realizations of the data. Since different iterations of the smoothing are correlated, one cannot simply combine them. Instead, we choose for each realization the one with the lowest $\Delta\chi^2$. We then calculate, for each realization, the likelihood of $\Omega_{k,0} \pm \sigma_{\Omega_{k,0}}$. For a given value of the significance α , we want to measure p_I and p_{II} , assuming a Gaussian likelihood for $\Omega_{k,0}$, i.e., $p_I = 2P(X > |\Omega_{k,0}|)$, and $p_{II} = 1 - 2P(X > |\Omega_{k,0}|)$. The results are reported on Table 2. While the probabilities of type I errors are reasonable, for a given α , the probability of type II errors are typically 40% ($\alpha = 0.05$) to 60% ($\alpha = 0.01$). While a LSST 3 year+DESI 5 years survey is not sufficient to rule out flatness at a high confidence level for curvature values of 0.1, it is important to keep in mind that this is only using low-redshift data, and does not need any assumption regarding the dark energy model.

	Λ	$k\text{-}\Lambda$	PEDE	$k\text{-PEDE}$
α	p_I	p_{II}	p_I	p_{II}
0.05	0.068	0.363	0.065	0.334
0.01	0.016	0.595	0.014	0.548

Table 3: Probabilities of type I and type II errors for the four fiducial models.

6 Summary and Conclusion

We combined forecast BAO data for a DESI 5-year-like survey and a realistic forecast for LSST SNIa to assess the ability of the joint surveys to provide model-independent litmus tests of the flat Λ CDM model. For this purpose, we generated mock data for four cosmologies: flat Λ CDM a non-flat Λ CDM universe with $\Omega_{k,0} = 0.1$, and two examples of dynamical dark energy, the PEDE model, with $\Omega_{k,0} = 0$ and $\Omega_{k,0} = 0.1$.

We applied the iterative smoothing method to reconstruct the expansion history in a model-independent manner, only assuming flatness.

The expected quality of LSST SNIa will allow to reconstruct very accurately certain diagnostics such as $\mathcal{O}m$ and q . In addition, we quantify the ability of the joint surveys to constrain $c/H_0 r_d$. We then proceed to testing the FLRW metric, measuring Θ and \mathcal{O}_k . The combination of LSST 3-year and DESI 5-years will allow to constrain \mathcal{O}_k to within ~ 0.035 , and Θ to within 0.0075, with a spread due to the SNIa uncertainties of up to ± 0.1 and 0.03 respectively. It is worth noting that the credible interval on $\Omega_{k,0}$ reported by DESI DR1 is $(-0.078, 0.068)$ for the flat Λ CDM model without any external data. We show that with the expected five-year data accuracy, a model-independent precision on the curvature parameter will be competitive.

In the case of the $\Omega_{k,0} = 0.1$ universes, the flatness assumption of eq. (2.3) is now incorrect, which leads to a biased expansion history and inconsistent estimations of $c/H_0 r_d$ from our two methods. Therefore, $H_0 r_d$ itself can be seen as a curvature test. An inconsistency between the two estimates of $H_0 r_d$, or with $\mathcal{O}_k(z) = \text{constant}$ or $\Theta(z) = 1$ can just be interpreted either as evidence of departure from flatness, or inconsistency between the two data sets.

A Smooth Derivatives

An interesting property of smoothing is that the derivative of the smooth function can be readily obtained from the derivative of the smoothing kernel.

Suppose we observe a function $y_i = f(t) + \epsilon_i$, where $\epsilon \sim \mathcal{N}(0, \mathbf{C})$. We want to reconstruct the smooth function $\hat{f}(t)$ and its successive derivative $\hat{f}^{(i)}(t)$.

Since smoothing is essentially a convolution by a smoothing kernel, one can straightforwardly define the smooth reconstruction of the successive derivatives as

$$\hat{y}_{n+1}(t) = \hat{y}_n(t) + \frac{B(t)}{A(t)}, \quad (\text{A.1})$$

where

$$B = \boldsymbol{\delta y}_n \cdot \boldsymbol{C}^{-1} \cdot \boldsymbol{W}(t), \text{ and} \quad (\text{A.2})$$

$$A = \mathbb{1}^\top \cdot \boldsymbol{C}^{-1} \cdot \boldsymbol{W}(t). \quad (\text{A.3})$$

The first and second smooth derivatives is obtained by deriving the previous equation with respect to t :

$$\hat{y}'_{n+1}(t) = \hat{y}'_n(t) + \frac{B'}{A} - \frac{BA'}{A^2}, \quad (\text{A.4})$$

$$\hat{y}''_{n+1}(t) = \hat{y}''_n(t) + \frac{B''}{A} - \frac{2A'B' + A''B}{A^2} + \frac{2A'^2B}{A^3}, \quad (\text{A.5})$$

where

$$B' = \boldsymbol{\delta y}_n^\top \cdot \boldsymbol{C}^{-1} \cdot \boldsymbol{W}'(t), \quad (\text{A.6})$$

$$A' = \mathbb{1}^\top \cdot \boldsymbol{C}^{-1} \cdot \boldsymbol{W}'(t), \quad (\text{A.7})$$

$$B'' = \boldsymbol{\delta y}_n^\top \cdot \boldsymbol{C}^{-1} \cdot \boldsymbol{W}''(t), \text{ and} \quad (\text{A.8})$$

$$A'' = \mathbb{1}^\top \cdot \boldsymbol{C}^{-1} \cdot \boldsymbol{W}''(t). \quad (\text{A.9})$$

In this work, we apply the algorithm to the LSST simulated SNIa with $t = \ln(1+z)$.

B Error propagation

The errors are propagated using the usual formula: for $\boldsymbol{Y} = \boldsymbol{f}(\boldsymbol{X})$, the covariance \boldsymbol{C}_Y is given by

$$\boldsymbol{C}_Y = \boldsymbol{J}^\top \cdot \boldsymbol{C}_X \cdot \boldsymbol{J}, \quad (\text{B.1})$$

where \boldsymbol{J} is the Jacobian of \boldsymbol{f} , and \boldsymbol{Y} stands for $c/H_0 r_d$, Θ , or \mathcal{O}_k .

Since the correlation between two redshift bins in the BAO data is negligible, we can propagate the errors independently at fixed redshift z . We then have

$$\boldsymbol{C}_{c/H_0 r_d} = \boldsymbol{J}_{c/H_0 r_d}^\top \cdot \boldsymbol{C}_{\text{BAO}} \cdot \boldsymbol{J}_{c/H_0 r_d} \quad (\text{B.2})$$

where

$$\boldsymbol{J}_{c/H_0 r_d} = \begin{pmatrix} \frac{1}{\mathcal{D}(z)} & 0 \\ 0 & \frac{1}{\mathcal{D}'(z)} \end{pmatrix}. \quad (\text{B.3})$$

For Θ and \mathcal{O}_k , the covariance matrix is simply the variance. The variance of Θ is obtained by

$$\sigma_\Theta^2 = \boldsymbol{J}_\Theta^\top \cdot \boldsymbol{C}_{\text{BAO}} \cdot \boldsymbol{J}_\Theta, \quad (\text{B.4})$$

where

$$\boldsymbol{J}_\Theta = \Theta \begin{pmatrix} \frac{r_d}{d_M} \\ \frac{r_d}{d_H} \end{pmatrix}, \quad (\text{B.5})$$

and that of \mathcal{O}_k by

$$\sigma_{\mathcal{O}_k} = 2 \frac{\Theta}{\mathcal{D}^2} \sigma_{\Theta}. \quad (\text{B.6})$$

In all cases, the total χ^2 for reconstruction n is obtained by

$$\chi_n^2 = \chi_{\text{SN},n}^2 + \chi_{\text{BAO},n}^2. \quad (\text{B.7})$$

Acknowledgments

The authors thank Kushal Loda for constructive discussions. B. L. acknowledges the support of the National Research Foundation of Korea (NRF-2022R1F1A1076338 and RS-2023-00259422). A.M. thanks Richard Kessler and the LSST DESC TD team for the production of the LSST dataset. A. S. would like to acknowledge the support by National Research Foundation of Korea NRF2021M3F7A1082056 and the support of the Korea Institute for Advanced Study (KIAS) grant funded by the government of Korea.

References

- [1] PLANCK collaboration, Planck 2018 results. VI. Cosmological parameters, *Astron. Astrophys.* **641** (2020) A6.
- [2] D.J. Eisenstein, I. Zehavi, D.W. Hogg, R. Scoccimarro, M.R. Blanton, R.C. Nichol et al., *Detection of the Baryon Acoustic Peak in the Large-Scale Correlation Function of SDSS Luminous Red Galaxies*, *ApJ* **633** (2005) 560 [[astro-ph/0501171](#)].
- [3] S. Alam, M. Aubert, S. Avila et al., *Completed SDSS-IV extended Baryon Oscillation Spectroscopic Survey: Cosmological implications from two decades of spectroscopic surveys at the Apache Point Observatory*, *Phys. Rev. D* **103** (2021) 083533 [[2007.08991](#)].
- [4] DESI Collaboration, A.G. Adame et al., *DESI 2024 IV: Baryon Acoustic Oscillations from the Lyman Alpha Forest*, *arXiv e-prints* (2024) [[2404.03001](#)].
- [5] DESI Collaboration, A.G. Adame et al., *DESI 2024 VI: Cosmological Constraints from the Measurements of Baryon Acoustic Oscillations*, *arXiv e-prints* (2024) [[2404.03002](#)].
- [6] DESI Collaboration, A.G. Adame et al., *DESI 2024 III: Baryon Acoustic Oscillations from Galaxies and Quasars*, *arXiv e-prints* (2024) [[2404.03000](#)].
- [7] S. Perlmutter, G. Aldering, G. Goldhaber, R.A. Knop, P. Nugent et al., *Measurements of Ω and Λ from 42 High-Redshift Supernovae*, *Astrophys. J.* **517** (1999) 565 [[astro-ph/9812133](#)].
- [8] A.G. Riess, A.V. Filippenko, P. Challis, A. Clocchiatti, A. Diercks et al., *Observational Evidence from Supernovae for an Accelerating Universe and a Cosmological Constant* [[arXiv:astro-ph/9805201](#)], *Astron. J.* **116** (1998) 1009 [[astro-ph/9805201](#)].
- [9] M. Betoule et al., *Improved cosmological constraints from a joint analysis of the SDSS-II and SNLS supernova samples*, *Astron. Astrophys.* **568** (2014) A22 [[1401.4064](#)].
- [10] PAN-STARRS1 collaboration, The Complete Light-curve Sample of Spectroscopically Confirmed SNe Ia from Pan-STARRS1 and Cosmological Constraints from the Combined Pantheon Sample, *Astrophys. J.* **859** (2018) 101.
- [11] D. Brout et al., *The Pantheon+ Analysis: Cosmological Constraints*, *Astrophys. J.* **938** (2022) 110 [[2202.04077](#)].
- [12] P.K. Aluri et al., *Is the observable Universe consistent with the cosmological principle?*, *Class. Quant. Grav.* **40** (2023) 094001 [[2207.05765](#)].

- [13] L. Perivolaropoulos and F. Skara, *Challenges for Λ CDM: An update*, *New Astron. Rev.* **95** (2022) 101659 [2105.05208].
- [14] M. Kamionkowski and A.G. Riess, *The Hubble Tension and Early Dark Energy*, 2211.04492.
- [15] E. Di Valentino, O. Mena, S. Pan, L. Visinelli, W. Yang, A. Melchiorri et al., *In the realm of the Hubble tension—a review of solutions*, *Class. Quant. Grav.* **38** (2021) 153001 [2103.01183].
- [16] C. Krishnan, R. Mohayaee, E.O. Colgáin, M.M. Sheikh-Jabbari and L. Yin, *Does Hubble tension signal a breakdown in FLRW cosmology?*, *Class. Quant. Grav.* **38** (2021) 184001 [2105.09790].
- [17] E. Abdalla et al., *Cosmology intertwined: A review of the particle physics, astrophysics, and cosmology associated with the cosmological tensions and anomalies*, *JHEAp* **34** (2022) 49 [2203.06142].
- [18] C. Krishnan, R. Mohayaee, E.O. Colgáin, M.M. Sheikh-Jabbari and L. Yin, *Hints of FLRW breakdown from supernovae*, *Phys. Rev. D* **105** (2022) 063514 [2106.02532].
- [19] T.L. Smith, M. Lucca, V. Poulin, G.F. Abellan, L. Balkenhol, K. Benabed et al., *Hints of early dark energy in Planck, SPT, and ACT data: New physics or systematics?*, *Phys. Rev. D* **106** (2022) 043526 [2202.09379].
- [20] J. Sola Peracaula, *The cosmological constant problem and running vacuum in the expanding universe*, *Phil. Trans. Roy. Soc. Lond. A* **380** (2022) 20210182 [2203.13757].
- [21] G.-B. Zhao, M. Raveri, L. Pogosian, Y. Wang, R.G. Crittenden, W.J. Handley et al., *Dynamical dark energy in light of the latest observations*, *Nature Astronomy* **1** (2017) 627 [1701.08165].
- [22] K. Lodha, A. Shafieloo, R. Calderon, E. Linder, W. Sohn, J.L. Cervantes-Cota et al., *DESI 2024: Constraints on Physics-Focused Aspects of Dark Energy using DESI DR1 BAO Data*, *arXiv e-prints* (2024) arXiv:2405.13588 [2405.13588].
- [23] R. Calderon, K. Lodha, A. Shafieloo, E. Linder, W. Sohn, A. de Mattia et al., *DESI 2024: Reconstructing Dark Energy using Crossing Statistics with DESI DR1 BAO data*, *arXiv e-prints* (2024) arXiv:2405.04216 [2405.04216].
- [24] E. Di Valentino, A. Melchiorri and J. Silk, *Planck evidence for a closed Universe and a possible crisis for cosmology*, *Nature Astronomy* **4** (2020) 196 [1911.02087].
- [25] W. Handley, *Curvature tension: Evidence for a closed universe*, *"Phys. Rev. D"* **103** (2021) L041301 [1908.09139].
- [26] S. Vagnozzi, E. Di Valentino, S. Gariazzo, A. Melchiorri, O. Mena and J. Silk, *The galaxy power spectrum take on spatial curvature and cosmic concordance*, *Physics of the Dark Universe* **33** (2021) 100851 [2010.02230].
- [27] S. Vagnozzi, A. Loeb and M. Moresco, *Eppur è piatto? The Cosmic Chronometers Take on Spatial Curvature and Cosmic Concordance*, *ApJ* **908** (2021) 84 [2011.11645].
- [28] R.E. Keeley, A. Shafieloo, G.-B. Zhao, J.A. Vazquez and H. Koo, *Reconstructing the Universe: Testing the Mutual Consistency of the Pantheon and SDSS/eBOSS BAO Data Sets with Gaussian Processes*, *AJ* **161** (2021) 151 [2010.03234].
- [29] S.-g. Hwang, B. L’Huillier, R.E. Keeley, M.J. Jee and A. Shafieloo, *How to use GP: effects of the mean function and hyperparameter selection on Gaussian process regression*, *J. Cosmology Astropart. Phys.* **2023** (2023) 014 [2206.15081].
- [30] R.E. Keeley and A. Shafieloo, *Ruling Out New Physics at Low Redshift as a Solution to the H_0 Tension*, *Phys. Rev. Lett.* **131** (2023) 111002 [2206.08440].
- [31] B. L’Huillier and A. Shafieloo, *Model-independent test of the FLRW metric, the flatness of the Universe, and non-local estimation of H_0* , *J. Cosmology Astropart. Phys.* **2017** (2017) 015 [1606.06832].

- [32] A. Shafieloo, B. L’Huillier and A.A. Starobinsky, *Falsifying Λ CDM : Model-independent tests of the concordance model with eBOSS DR14Q and Pantheon*, *Phys. Rev. D* **98** (2018) 083526 [[1804.04320](#)].
- [33] D. Staicova and D. Benisty, *Constraining the dark energy models using baryon acoustic oscillations: An approach independent of $H_0 \cdot rd$* , *Astron. Astrophys.* **668** (2022) A135 [[2107.14129](#)].
- [34] D. Benisty, S. Pan, D. Staicova, E. Di Valentino and R.C. Nunes, *Late-Time constraints on Interacting Dark Energy: Analysis independent of H_0 , r_d and M_B* , [2403.00056](#).
- [35] DESI Collaboration, A. Aghamousa et al., *The DESI Experiment Part I: Science, Targeting, and Survey Design*, *arXiv e-prints* (2016) arXiv:1611.00036 [[1611.00036](#)].
- [36] LSST DARK ENERGY SCIENCE collaboration, *Using Host Galaxy Photometric Redshifts to Improve Cosmological Constraints with Type Ia Supernovae in the LSST Era*, *Astrophys. J.* **944** (2023) 212 [[2210.07560](#)].
- [37] X. Li and A. Shafieloo, *A Simple Phenomenological Emergent Dark Energy Model can Resolve the Hubble Tension*, *ApJ* **883** (2019) L3 [[1906.08275](#)].
- [38] LSST collaboration, *LSST: from Science Drivers to Reference Design and Anticipated Data Products*, *Astrophys. J.* **873** (2019) 111 [[0805.2366](#)].
- [39] R. Kessler, J.P. Bernstein, D. Cinabro, B. Dilday, J.A. Frieman, S. Jha et al., *SNANA: A Public Software Package for Supernova Analysis*, *Publ. Astron. Soc. Pac.* **121** (2009) 1028 [[0908.4280](#)].
- [40] THE PLASTiCC TEAM collaboration, *The Photometric LSST Astronomical Time-series Classification Challenge (PLASTiCC): Data set*, *arXiv:1810.00001* (2018) .
- [41] R.S. de Jong, O. Agertz, A.A. Berbel, J. Aird, D.A. Alexander et al., *4MOST: Project overview and information for the First Call for Proposals*, *The Messenger* **175** (2019) 3 [[1903.02464](#)].
- [42] R. Kessler, D. Cinabro, B. Bassett, B. Dilday, J.A. Frieman et al., *Photometric Estimates of Redshifts and Distance Moduli for Type Ia Supernovae*, *Astrophys. J.* **717** (2010) 40 [[1001.0738](#)].
- [43] M.L. Graham, A.J. Connolly, Ž. Ivezić, S.J. Schmidt, R.L. Jones, M. Jurić et al., *Photometric Redshifts with the LSST: Evaluating Survey Observing Strategies*, *Astron. J.* **155** (2018) 1 [[1706.09507](#)].
- [44] LSST DARK ENERGY SCIENCE collaboration, *The LSST Dark Energy Science Collaboration (DESC) Science Requirements Document*, *arXiv:1809.01669* (2018) [[1809.01669](#)].
- [45] C. Clarkson, B. Bassett and T.H.-C. Lu, *A General Test of the Copernican Principle*, *Physical Review Letters* **101** (2008) 011301 [[0712.3457](#)].
- [46] A. Shafieloo and C. Clarkson, *Model independent tests of the standard cosmological model*, *Phys. Rev. D* **81** (2010) 083537 [[0911.4858](#)].
- [47] V. Sahni, A. Shafieloo and A.A. Starobinsky, *Two new diagnostics of dark energy*, *Phys. Rev. D* **78** (2008) 103502 [[0807.3548](#)].
- [48] A. Shafieloo, U. Alam, V. Sahni and A.A. Starobinsky, *Smoothing supernova data to reconstruct the expansion history of the Universe and its age*, *MNRAS* **366** (2006) 1081 [[astro-ph/0505329](#)].
- [49] A. Shafieloo, *Model-independent reconstruction of the expansion history of the Universe and the properties of dark energy*, *MNRAS* **380** (2007) 1573 [[astro-ph/0703034](#)].
- [50] B. L’Huillier, A. Shafieloo and H. Kim, *Model-independent cosmological constraints from growth and expansion*, *MNRAS* **476** (2018) 3263 [[1712.04865](#)].

- [51] H. Koo, A. Shafieloo, R.E. Keeley and B. L'Huillier, *Model-independent Constraints on Type Ia Supernova Light-curve Hyperparameters and Reconstructions of the Expansion History of the Universe*, [ApJ **899** \(2020\) 9 \[2001.10887\]](#).
- [52] H. Koo, A. Shafieloo, R.E. Keeley and B. L'Huillier, *Model selection and parameter estimation using the iterative smoothing method*, [J. Cosmology Astropart. Phys. **2021** \(2021\) 034 \[2009.12045\]](#).
- [53] H. Koo, R.E. Keeley, A. Shafieloo and B. L'Huillier, *Bayesian vs frequentist: comparing Bayesian model selection with a frequentist approach using the iterative smoothing method*, [J. Cosmology Astropart. Phys. **2022** \(2022\) 047 \[2110.10977\]](#).